Supplemental Figure 1

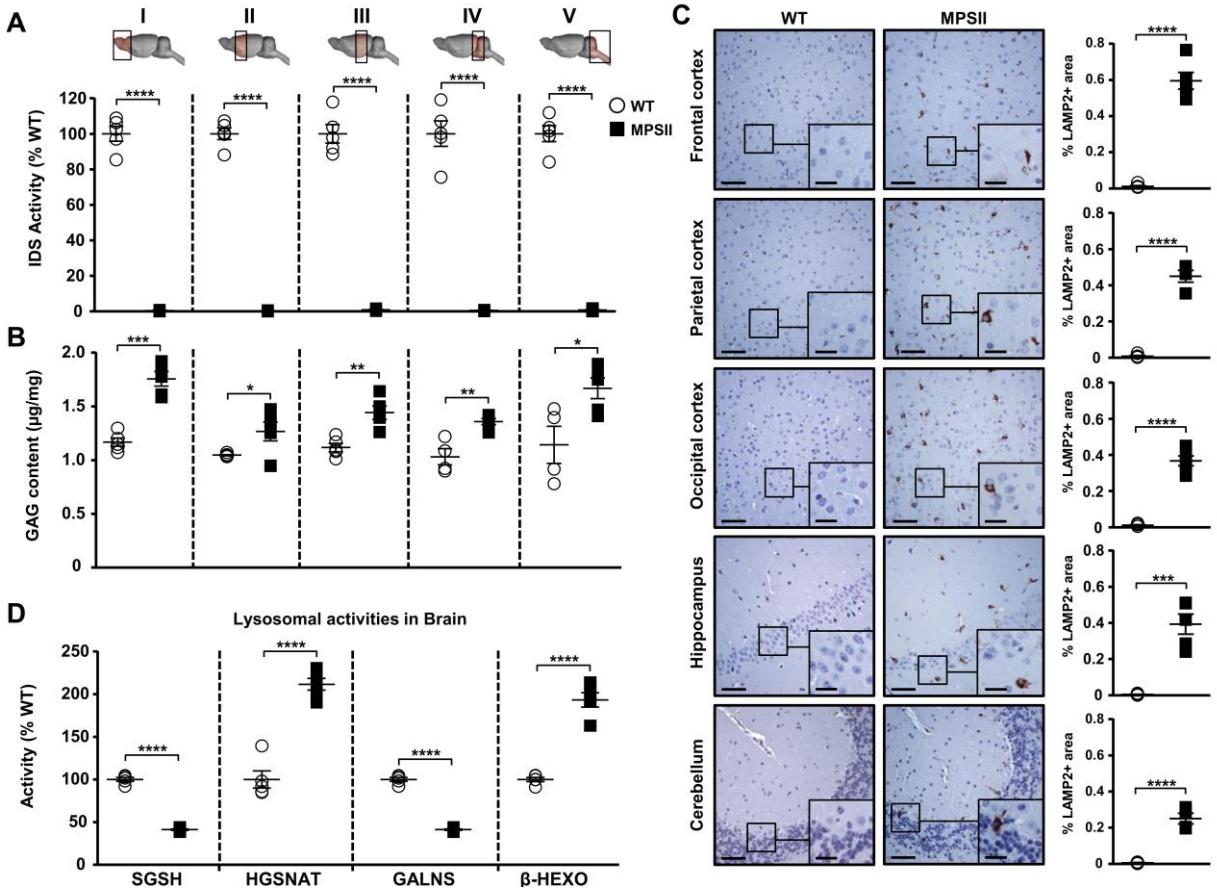

Supplemental Figure 1. Characterization of CNS lysosomal pathology in 2-month-old IDS-deficient mice. (**A**) Measurement of IDS activity in brain extracts from wild-type (WT) and IDS-deficient males. IDS activity was practically undetectable in IDS-deficient mice. (**B**) Quantification of GAG content in tissue extracts obtained from different sections of the encephalon. At 2 months of age, IDS-deficient mice presented pathological accumulation of GAGs in all regions analysed. (**C**) Immunostaining for the lysosomal marker LAMP2 of brain tissue sections. The encephalon of IDS-deficient males showed cells with intense LAMP2 staining, indicative of enlargement of the lysosomal compartment. Scale bars are 50 µm, and 20 µm for insets. Histograms represent the quantification of the percentage of LAMP2+ area in each region. (**D**) Measurement of the activity of other lysosomal enzymes in brain extracts. The activity of the enzymes SGSH, HGSNAT, GALNS and β-HEXO was significantly altered in the brains of IDS-deficient males. Data are shown as mean ± SEM of 4-5 animals/group. **P*<0.05, ***P*<0.01, ****P*<0.001 and *****P*<0.0001 *vs.* WT.

Supplemental Figure 2

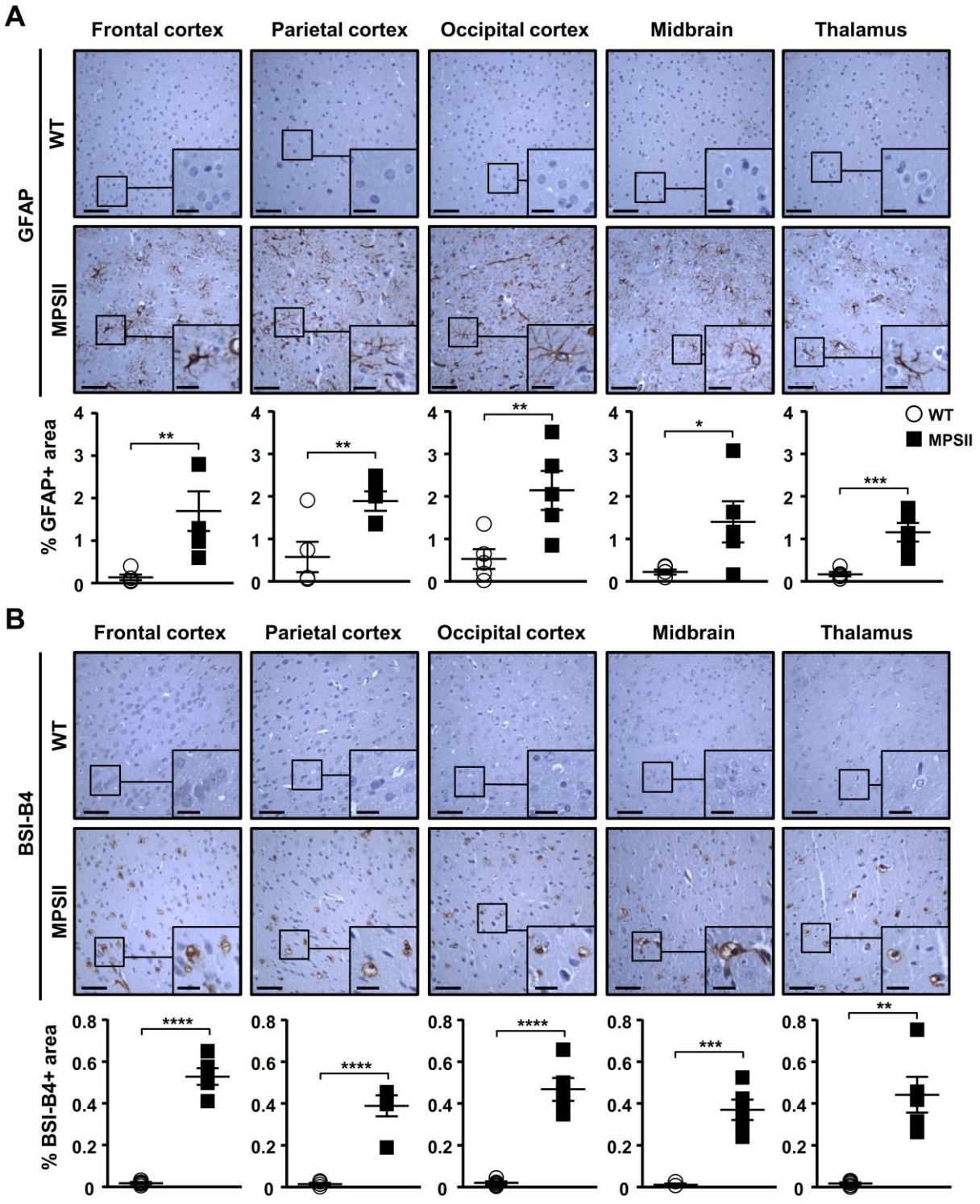

Supplemental Figure 2. Neuroinflamation in 2-month-old IDS-deficient mice. (**A-B**) Immunostaining of paraffin sections of the encephalon of wild-type (WT) and IDS-deficient mice with anti-GFAP antibody (**A**) or BSI-B4 lectin (**B**). Histograms represent the quantification of the percentage of GFAP+ or BSI-B4+ area in each region. IDS-deficient mice showed signs of astrogliosis and microgliosis in all the encephalon areas analysed. Scale bars are 50 µm, and 20 µm for insets. Values are means ± SEM of 4-5 animals/group. **P*<0.05, ***P*<0.01, ****P*<0.001 and *****P*<0.0001 *vs.* WT.

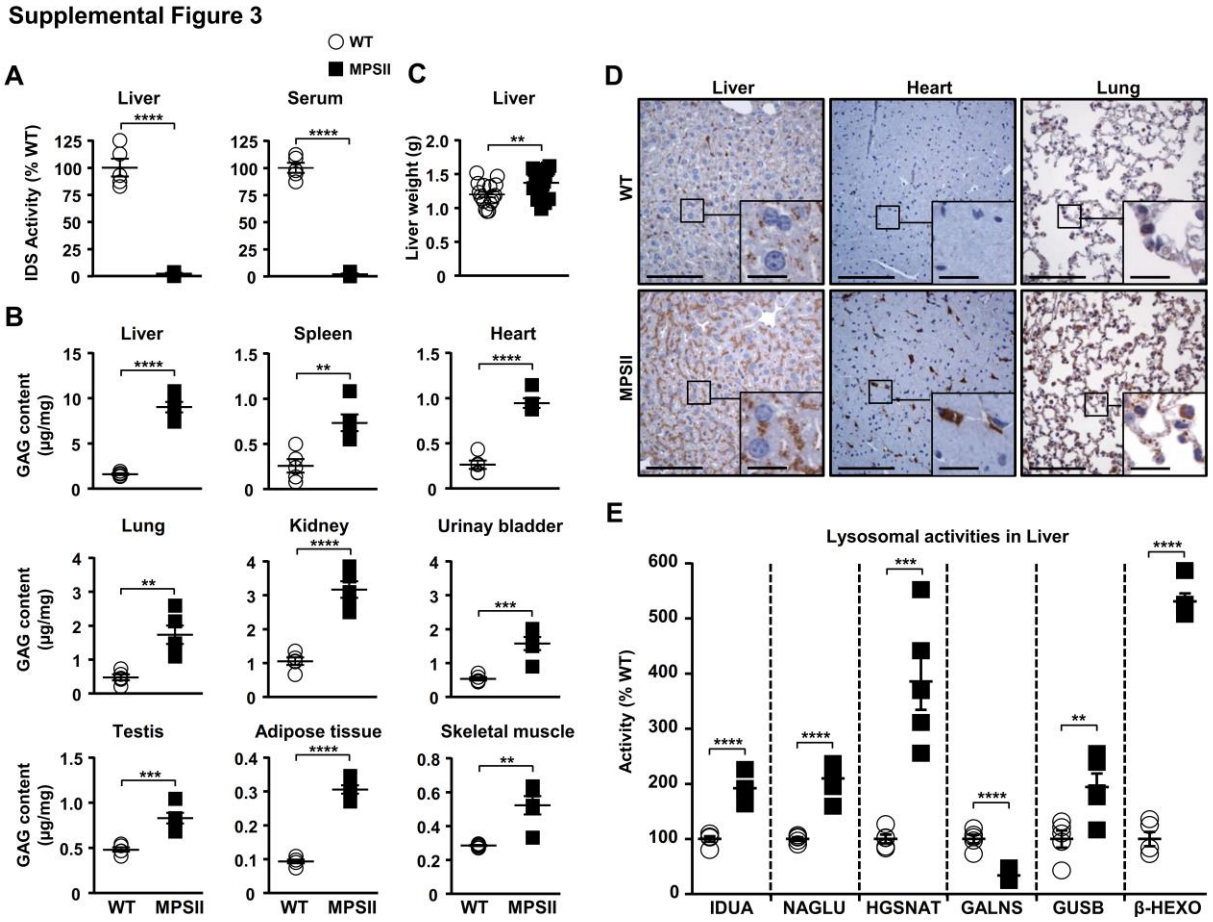

Supplemental Figure 3. Characterization of somatic pathology in 2-month-old MPSII mice. (**A**) Measurement of IDS activity in liver extracts and serums from wild-type (WT) and MPSII males. IDS activity was practically undetectable in IDS-deficient mice. (**B**) Glycosaminoglycan (GAG) storage in somatic tissues. At 2 months of age, IDS-deficient mice presented considerable GAG accumulation in somatic organs, particularly in the liver. (**C**) Wet weight of the liver showing a slight increase in the weight of the organ in IDS-deficient mice. (**D**) Immunostaining of somatic tissue sections with the lysosomal marker LAMP1. Scale bars are 100 µm, and 20 µm for insets. (**E**) Measurement of the enzymatic activity of other lysosomal enzymes such as IDUA, NAGLU, HGSNAT, GALNS, GUSB and β-HEXO in liver extracts. Data are shown as mean ± SEM of 4-5 animals/group for (**A**), (**B**), (**D**), (**E**), and 17-18 animals/group for (**C**). ***P*<0.01, ****P*<0.001 and *****P*<0.0001 *vs.* WT.

Supplemental Figure 4

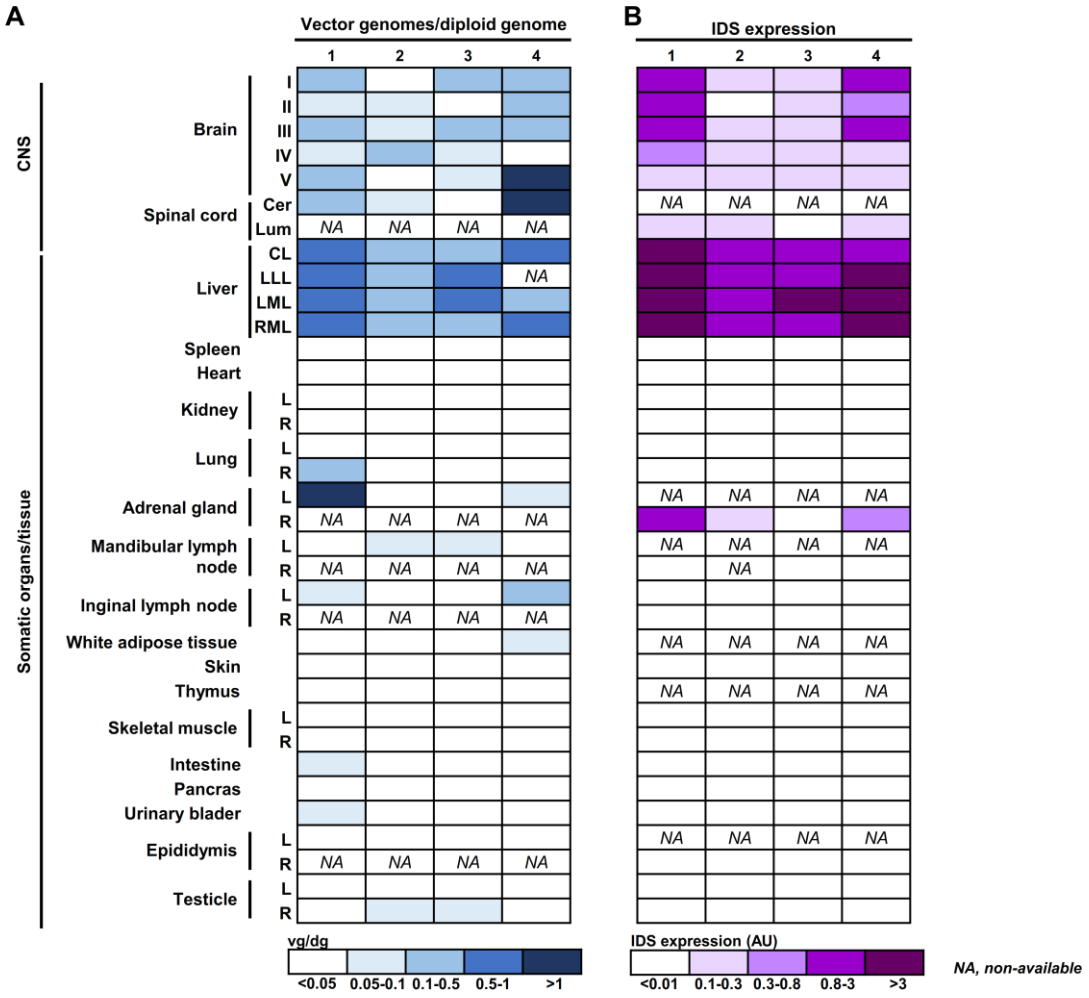

Supplemental Figure 4. Biodistribution of AAV9-*Ids* vectors and *Ids* expression following intra-CSF delivery to MPSII mice. (A) Vector genome copy number per diploid genome and (**B**) *Ids* mRNA expression two months after intra-CSF AAV9-*Ids* administration of $5x10^{10}$ vg to 2-month-old MPSII mice. The encephalon was sliced in 5 coronal sections (I-V). Cer, cervical; Lum, lumbar; CL, caudate lobe; LLL, left lateral lobe; LML, left medial lobe; RML, right medial lobe; L, left; R, right; AU, arbitrary unit; *NA*, non-available.

Supplemental Figure 5

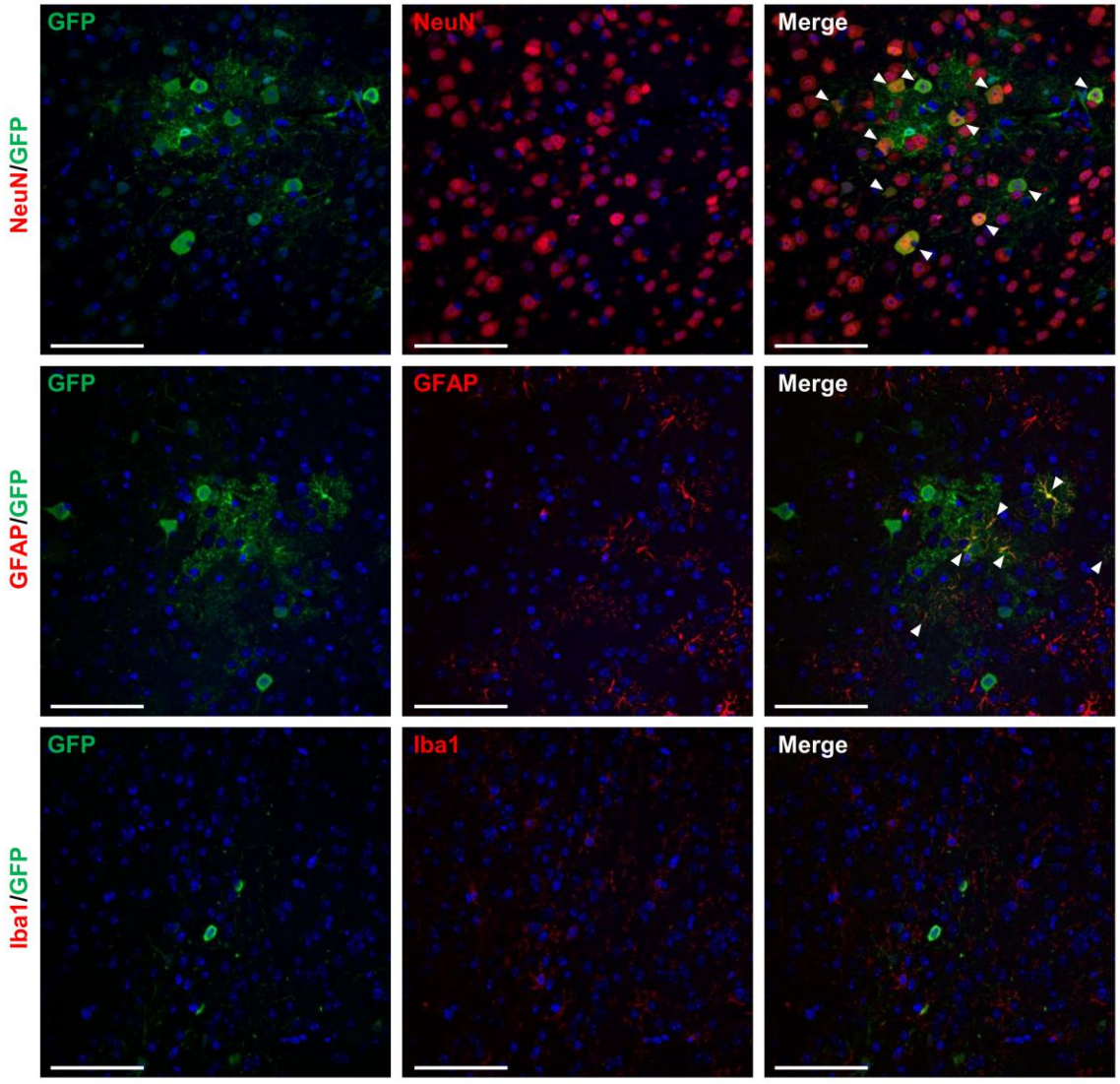

Supplemental Figure 5. AAV9 transduces predominantly neurons following intra-CSF delivery to mice. Co-localization study on brain sections from 8-week-old MPSII mice administered intra-CSF with $5x10^{10}$ vg of AAV9-GFP vector and analysed 10 days post-injection. Tissue sections were double-immunostained for GFP (*green*) and specific markers (*red*) for neurons (NeuN, *top panels*), astrocytes (GFAP, *central panels*) or microglia (Iba1, *bottom panels*). Nuclei were counterstained with Hoechst. Confocal microscopy images showed efficient transduction of neurons, occasional transduction of astrocytes and no transduction of microglia after intra-CSF AAV9-GFP delivery to mice. Arrowheads indicate double-positive cells. Scale bars are 100 µm.

Supplemental Figure 6

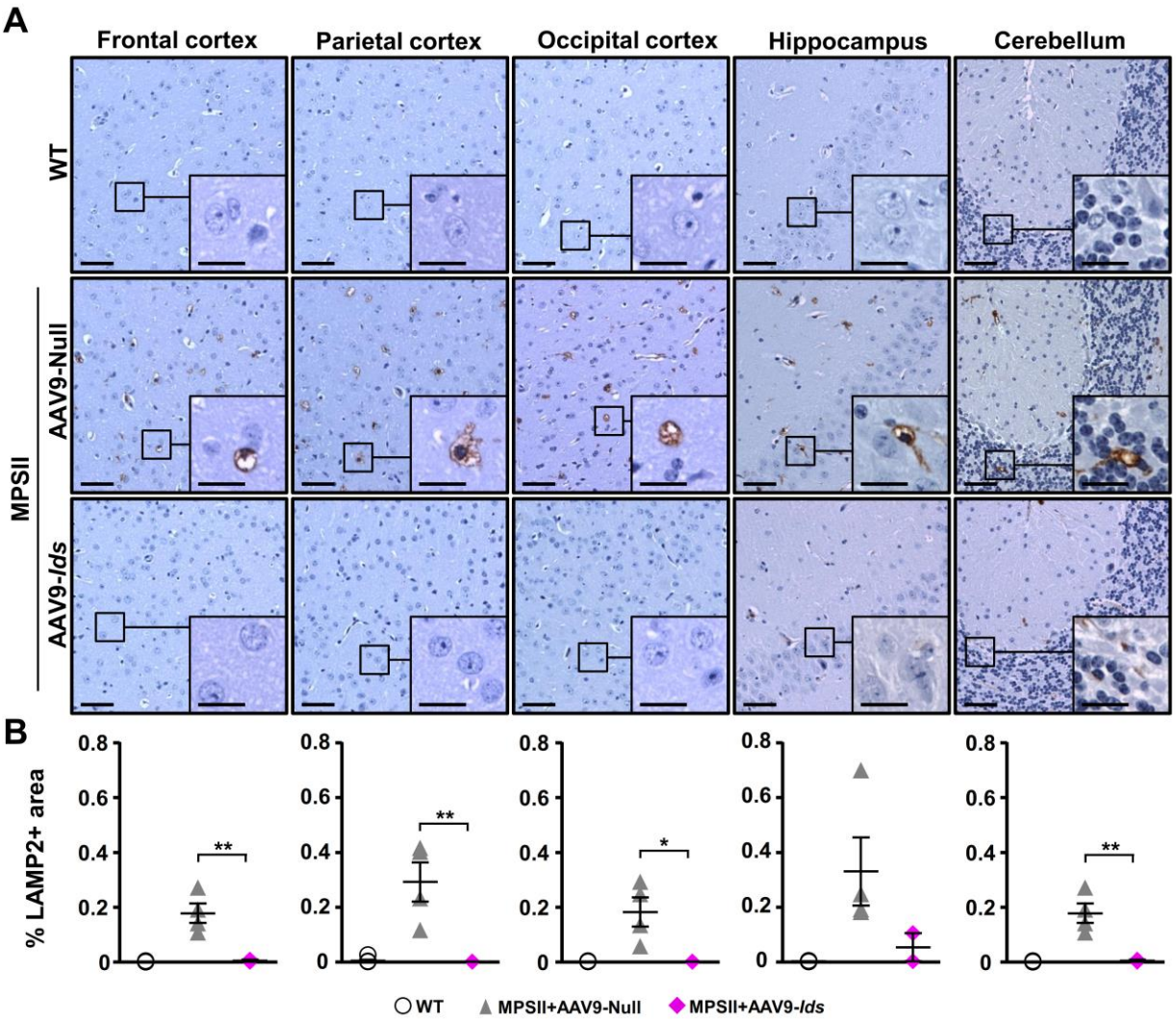

Supplemental Figure 6. Long-term correction of lysosomal distention in the CNS of MSPII mice by intra-CSF AAV9-*Ids* delivery. Immunohistochemistry for the lysosomal marker LAMP2 in different brain areas from wild-type (WT), and MPII mice administered in the CSF with null (MPSII+AAV9-Null) or IDS-encoding AAV9 vectors (MPSII+AAV9-*Ids*) 8 months after vector delivery (i.e. at 10 months of age). (**A**) Representative photomicrographs of LAMP2 immunostaining in different brain regions. Scale bars are 50 µm, and 20 µm for insets. (**B**) Histograms represent the quantification of the percentage of LAMP2+ area in each brain area. Results are shown as means ± SEM of 2-6 animals/group. **P*<0.05 and ***P*<0.01 vs. MPSII+AAV9-Null.

Supplemental Figure 7

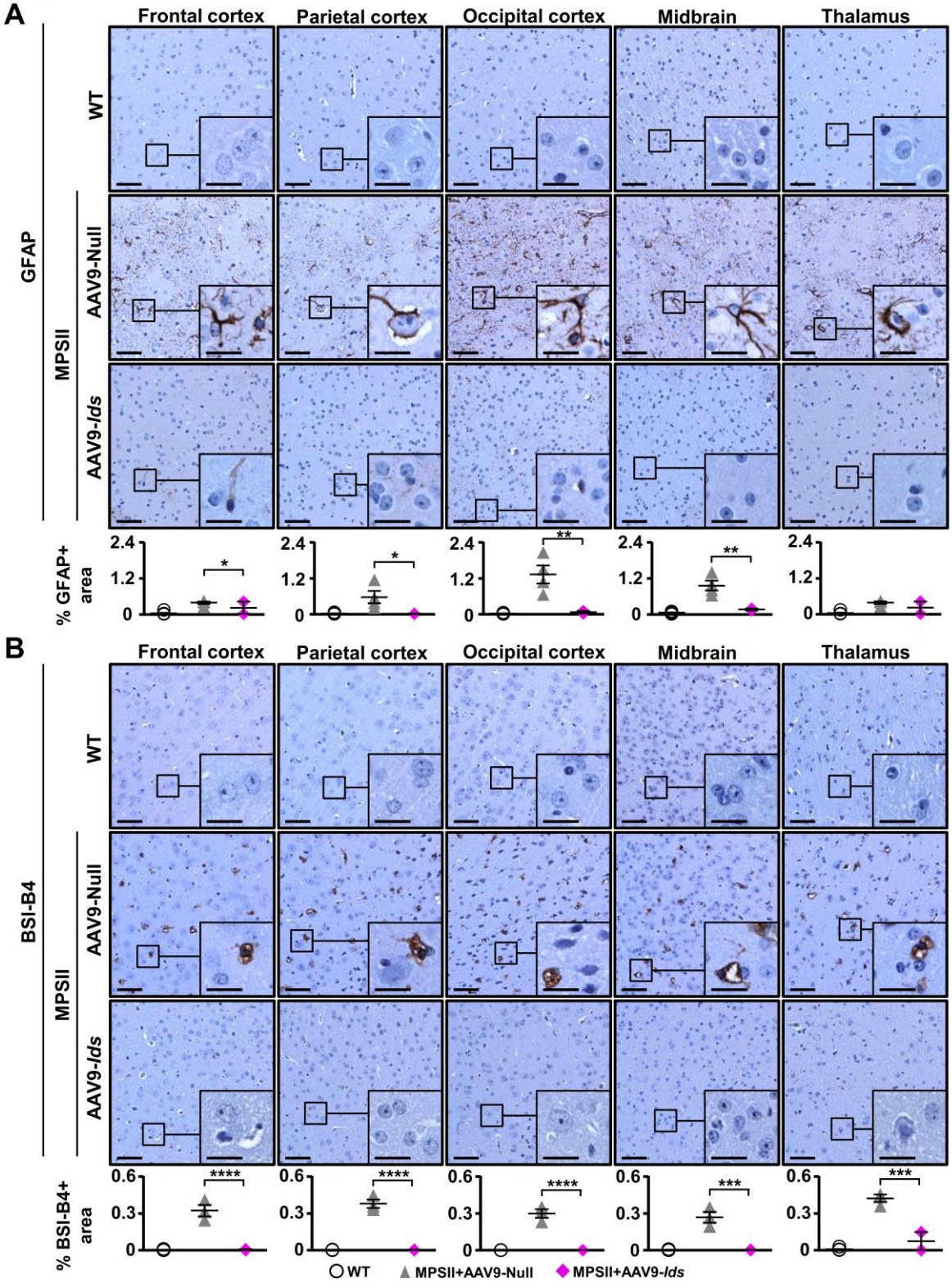

Supplemental Figure 7. Long-term correction of CNS neuroinflamation in MPSII mice after intra-CSF AAV9-*Ids* administration. Neuroinflammation evaluation in different brain sections from healthy wild-type (WT) or MPSII mice injected in the cisterna magna with either Null vector (MPSII+AAV9-Null) or therapeutic vector (MPSII+AAV9-*Ids*) 8 months after vector administration (i.e. at 10 months of age). (**A**) Representative micrographs of GFAP immunostaining, a marker of astrocytosis, in different areas of the brain. (**B**) Representative

photomicrographs of the staining with the microglial marker BSI-B4 in different brain regions. Scale bars are 50 µm, 20 µm for insets. Histograms depicted the percentage of GFAP or BSI-B4 positive area quantified in each brain section. Data are shown as means ± SEM of 2-6 animals/group. *P<0.05, **P<0.01, ***P<0.001 and ****P<0.0001 vs. MPSII+AAV9-Null.

Supplemental Table 1. List of genes differentially expressed in untreated and treated MPSII mice.

	Fold Change *vs*. WT			Fold Change *vs*. WT	
Gene Symbol	**AAV9-*Ids***	**AAV9-Null**	**Gene Symbol**	**AAV9-*Ids***	**AAV9-Null**
Cd68	1.16	2.49	Ctsd	1.04	1.45
LOC101055995	1.73	0.24	5930403L14Rik	1.29	1.75
C3ar1	0.98	2.52	Iglv1	1.38	2.79
Ccl3	0.98	2.95	Hexb	1.10	1.63
Tlr13	0.92	2.31	Astl	0.74	0.50
Tyrobp	0.93	2.05	Ptpn6	1.22	1.54
Gpnmb	1.15	2.17	Olfr152	1.31	0.66
Lag3	1.26	2.23	Pla2g2d	0.91	0.59
C1qa	1.05	1.85	Defa-rs1	1.45	0.74
Emr1	0.92	1.87	D930048G16Rik	0.64	1.13
Lyz2	1.32	3.02	Cd33	1.09	1.78
Plek	0.93	1.78	Olfr544	1.00	0.61
Pros1	1.23	1.85	C4b	1.22	2.15
Fcrls	1.42	2.60	LOC102638562	1.21	0.76
Lilrb4	1.57	2.93	Cd109	1.04	1.49
Ctss	1.22	2.20	Tmem254b	1.82	1.95
C1qc	0.99	1.86	Fcer1g	0.86	1.70
Ctsz	0.94	1.53	Cpne3	1.17	1.45
C1qb	1.20	2.21	Gm4832	1.02	1.53
Ifi44	1.70	2.10	Gm11009	0.69	0.58
Foxe3	0.54	0.68	Aqp4	1.28	1.46
Ces2d-ps	1.12	0.55	Taf11	0.86	1.27
Ifnb1	0.65	0.64	I830077J02Rik	1.22	1.90
Gfap	1.26	2.38	Gm14484	0.79	0.59
Zfp599	1.07	1.60	Brca2	0.94	1.44
Mpeg1	1.23	2.69	Gm15462	1.04	0.57
Gimap8	1.71	1.22	Kdr	1.15	1.55
Decr2	0.88	1.37	9230116N13Rik	0.66	0.80
1700120C14Rik	1.32	2.45	Slc7a11	1.24	1.59
Prss41	1.10	0.59	Cd180	1.07	1.66
Unc93b1	1.19	1.76	Gusb	0.84	1.23
Traj12	1.08	0.47	Rnaset2a	1.02	1.33
Fxyd4	1.44	0.72	Gm11725	1.33	0.89
Gm17421	1.20	0.72	Klk7	0.79	0.68
Slc22a27	1.13	1.74	Olfr507	1.05	0.53
Ifitm3	1.25	1.54	Trbv13-1	1.43	0.82
Eci1	0.82	1.42	Hpse	1.05	1.87
Trem2	1.05	2.10	Iqcf5	0.73	0.53
Csf3r	1.01	1.57	Hbq1a	0.66	0.47
Cyba	1.05	1.66	Gm12127	1.77	1.04
Olfr91	0.61	0.72	Gm11646	1.39	1.31
Gm10134	0.94	1.69	Lgals9	1.00	1.54
Gm5724	1.18	1.64	Thbs4	1.16	1.58
Havcr2	1.09	1.69	Cd63	1.09	1.45
Grid1	1.19	1.45			

Results for AAV9-*Ids* and AAV9-Null groups are shown as a fold-change *vs*. WT levels.